

See discussions, stats, and author profiles for this publication at:
<https://www.researchgate.net/publication/226852708>

Conformational differences of oxytocin and vasopressin as observed by fluorescence anisotropy decays and transient effects in collisional quenching of tyrosine fluorescence

ARTICLE *in* JOURNAL OF FLUORESCENCE · JANUARY 1991

Impact Factor: 1.93 · DOI: 10.1007/BF00865363

CITATIONS

11

READS

24

7 AUTHORS, INCLUDING:



Ignacy Gryczynski

University of North Texas HSC at Fort W...

367 PUBLICATIONS 9,395 CITATIONS

SEE PROFILE



Joseph R Lakowicz

University of Maryland Medical Center

878 PUBLICATIONS 42,255 CITATIONS

SEE PROFILE

Conformational Differences of Oxytocin and Vasopressin as Observed by Fluorescence Anisotropy Decays and Transient Effects in Collisional Quenching of Tyrosine Fluorescence¹

Ignacy Gryczynski,² Henryk Szmacinski,² Gabor Laczko,² Wieslaw Wiczk,² Michael L. Johnson,³ Jozef Kusba,² and Joseph R. Lakowicz²

Received November 21, 1990; accepted December 18, 1990

We used gigahertz frequency-domain fluorometry to examine the tyrosyl fluorescence intensity and anisotropy decays of the single-tyrosine cyclic peptide hormones oxytocin and vasopressin. Acrylamide quenching and a distance-dependent quenching model for collisional quenching were used to evaluate the extent of tyrosyl exposure to the quencher and to provide increased resolution of the picosecond anisotropy decays. Analysis of the intensity decays using a lifetime distribution model shows different distributions for oxytocin and vasopressin. We found that the tyrosyl fluorescence of lysine-vasopressin, as revealed both by the lifetime Stern-Volmer plots and from the quenching analysis, is quenched more effectively than oxytocin. For *N*-acetyltyrosinamide (NATyrA), oxytocin, and lysine-vasopressin, we recovered apparent diffusion coefficients for quenching of 4.7×10^{-6} , 0.44×10^{-6} , and $4.3 \times 10^{-6} \text{ cm}^2/\text{s}$, respectively, the lower value for oxytocin suggesting a shielded environment for its tyrosyl residue. Tyrosyl anisotropy decays were recovered by global analysis of progressively quenched samples. Compared with oxytocin, vasopressin displayed a longer correlation time for overall rotational diffusion and a higher amplitude for picosecond segmented motions of its tyrosyl residue. All the data are consistent with a more extended and flexible solution structure for vasopressin than for oxytocin.

KEY WORDS: Oxytocin; vasopressin; fluorescence intensity; fluorescence anisotropy decays; tyrosine fluorescence; collisional quenching.

INTRODUCTION

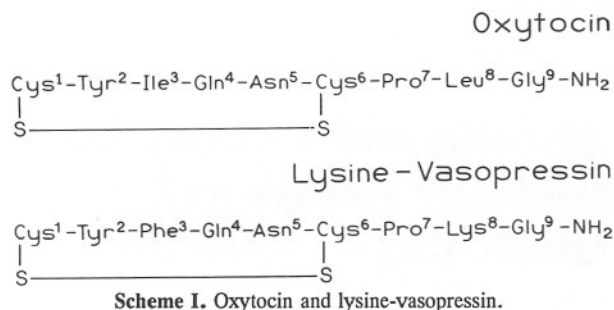
The peptide hormones oxytocin and lysine vasopressin each display unique physiological actions. Oxytocin stimulates smooth muscle and uterine contraction,

and vasopressin is an antidiuretic and a vasoconstrictor. Despite their distinct physiological actions, their structures are similar (Scheme I). Both contain a cyclic hexapeptide closed via a disulfide bridge and a noncyclic region containing three amino acids. Each contains a single tyrosine residue at position 2, which is used as the intrinsic fluorescent probe in the current study. The peptide hormones differ in sequence at position 3, where a phenylalanine residue in vasopressin replaces the isoleucine residue in oxytocin. The only other difference is the presence of a lysine at site 8 in vasopressin (lysine-vasopressin), replacing a leucine in oxytocin.

¹ Dedicated to Professor Alfons Kawski on the occasion of his 65th birthday.

² Center for the Fluorescence Spectroscopy and Department of Biological Chemistry, University of Maryland, School of Medicine, 660 West Redwood Street, Baltimore, Maryland 21201.

³ Department of Pharmacology, University of Virginia, Charlottesville, Virginia 22908.



The similar structures, but distinct physiological activities, of these peptides have resulted in a large number of studies to characterize their structure and dynamics [1–4]. The physical studies of oxytocin and vasopressin all suggest that, in solution, oxytocin is more compact than vasopressin. For instance, oxytocin was found to permeate thin films more rapidly than vasopressin [5], and it has not been possible to grow crystals of vasopressin presumably due to its flexibility and conformational variability [6]. Crystal structures have been reported for desamino oxytocin [7] and for the cyclic pressin region of vasopressin, i.e., a fragment lacking the carboxy-terminal tripeptide [8]. It has been proposed [9] that the phenol ring is positioned against the cyclic ring system in oxytocin, and points away from this ring system in vasopressin, and is thus exposed to the aqueous phase.

Fluorescence spectroscopy allows a comparison of the solution properties of oxytocin and vasopressin. Each hormone contains a single tyrosine residue which can serve as an intrinsic probe for peptide conformation and dynamics [10]. However, it has been difficult to take advantage of this probe because tyrosine absorbs and emits in the ultraviolet, displays a small separation between absorption and emission (Stokes' shift) and displays decay times in the range of 1–3 ns. Consequently, only a few laboratories have carried out detailed studies of the time-dependent decays of tyrosyl peptides and proteins [4,11,12].

In recent years there have been remarkable advances in instrumentation for the resolution of complex time-dependent emissions. These advances include improved instrumentation for time-domain [13–20] and frequency-domain measurements [21–24] of intensity and anisotropy decays. Additionally, the method of global analysis has provided increased resolution of multiexponential and/or complex decay process by the combination of several experimental data sets to recover the parameters which describe a single phenomenon [12,

25–27]. These advances in instrumentation and analysis have increased the potential of fluorescence methods for detailed evaluation of the structure and dynamics of biological macromolecules.

We used the frequency-domain method, and global analysis in the presence of quenching, to investigate the anisotropy decays of oxytocin and vasopressin and to recover the parameters characteristic of transient effects in quenching. The use of fluorescence anisotropy decays for studies of protein dynamics is widely understood, but the use of quenching during the anisotropy measurements is less familiar. We obtained increased resolution of the picosecond motions of oxytocin and vasopressin by global analysis in the presence of acrylamide quenching. By quenching we are able to decrease the mean decay time and, thereby, vary the natural time window of the observations [28]. More specifically, the overall hydrodynamic rotations contribute more to the anisotropy data when the decay time is longer, and the segmental motions of the fluorescent residue are more evident in the anisotropy data when the decay time is reduced by quenching. Acrylamide was used as a quencher because it is polar, is unchanged, and does not appear to interact with proteins [29]. Acrylamide is commonly used as a quencher of tryptophan fluorescence [28–33] but only rarely used as a tyrosine quencher [34] due to the high screening effect of acrylamide on the tyrosine absorption spectrum, which makes steady-state intensity measurements difficult due to the corrections needed for the inner filter effect. This difficulty is not present in time-resolved measurements, in either the time or the frequency domain, because the intensity and anisotropy decays are not affected by inner filter effects.

In the present paper we also describe transient effects in the time-dependent quenching of tyrosine and the tyrosyl peptide hormones. It is now known that collisional quenching results in nonexponential decays of the fluorescence intensity [35–39]. Such effects are known to result from a rapid extinction of fluorophore–quencher pairs soon after excitation, followed by diffusion-limited quenching at longer times [40,41]. Such effects have now been observed in single tryptophan proteins [42]. In the present report, we analyze the data in terms of two models for transient effects, the radiation boundary condition (RBC)⁴ model and the distance-dependent quenching (DDQ) model. Both models can reveal the fluorophore–quencher interaction radius (a) and the mu-

⁴ Abbreviations used: NATyrA, *N*-acetyltyrosinamide; DDQ, distance-dependent quenching; DODCI, 3'3'-diethyl-2,2'-oxadicarbo-cyanine iodide; RBC, radiation boundary condition model for quenching; vasopressin, lysine-vasopressin.

tual diffusion coefficient (D). In the RBC model quenching is assumed to occur only at the interaction radius (a) with a specific rate constant for quenching (κ). The value of κ is the rate of fluorophore deactivation when a quencher is present at the interaction radius. In the DDQ model, the rate constant for quenching is assumed to decrease exponentially with distance and, thus, reflect electron-exchange, charge transfer, or Dexter-like interactions [74]. However, we do not have a usable model for collisional quenching in the sterically hindered and anisotropic environment around a protein. Hence, the values of D and a are apparent values, which appear to reflect the degree of exposure of the fluorescent residue to the aqueous phase [19]. This is the first report in which we used the distance-dependent quenching model. Further experimentation and analysis are needed to understand the factors which influence k_a .

THEORY AND CALCULATIONS

Multiexponential Decays

Fluorescence intensity decays can be described as the sum of exponentials

$$I(t) = \sum_i \alpha_i e^{-t/\tau_i} \quad (1)$$

where τ_i are the individual decay times and α_i the associated preexponential factors. The fractional contribution of the i th component to the total fluorescence is

$$f_i = \frac{\alpha_i \tau_i}{\sum_j \alpha_j \tau_j} \quad (2)$$

where $\Sigma f_i = 1$. Since the frequency-domain data are collected without regard for the total intensity, it is also customary to normalize the α_i values, i.e., $\Sigma \alpha_i = 1$.

Lifetime Distributions

The intensity decays can also be described by lifetime distributions, in which the amplitudes α_i are continuous distributions in τ , i.e., $\alpha(\tau)$ [43–46]. The intensity decay then contains components for each lifetime τ with an amplitude $\alpha(\tau)$. The component with each individual τ value is given by

$$I(\tau, t) = \alpha(\tau) e^{-t/\tau} \quad (3)$$

The total decay law is the sum

$$I(t) = \int_{\tau=0}^{\infty} \alpha(\tau) e^{-t/\tau} d\tau \quad (4)$$

By analogy with the multiexponential model, the $\alpha(\tau)$ distribution can be multimodal:

$$\alpha(\tau) = \sum_i g_i \alpha_i^0(\tau) = \sum_i \alpha_i(\tau) \quad (5)$$

where i refers to the i th component of the distribution centered at $\bar{\tau}_i$ and g_i represents the amplitude of this component. The g_i values are the amplitude factors and $\alpha_i^0(\tau)$ the normalized shape factors, i.e., $\int_0^{\infty} \alpha_i^0(\tau) d\tau = 1.0$ for each mode of the distribution. We arbitrarily selected Lorentzian distributions for each component. For this function $\alpha(\tau)$ is given by

$$\alpha_L(\tau) = \frac{1}{\pi} \cdot \frac{\Gamma/2}{(\tau - \bar{\tau})^2 + (\Gamma/2)^2} \quad (6)$$

where $\bar{\tau}$ is the central value of the distribution and Γ the full-width at half-maximum (hw). An alternative approach would be to use $\alpha(\tau)$ distributions which are not described by any particular function. This approach may be superior because it makes no assumption about the shape of the distribution. However, the use of functional form for $\alpha(\tau)$ minimizes the number of floating parameters, which in turn allows stable fits to the data.

We define $\alpha_i(\tau)$ as the integrated preexponential factor for each component. For any distribution the preexponential factor for the i th mode is given by

$$\alpha_i = \frac{\int_0^{\infty} \alpha_i(\tau) d\tau}{\int_0^{\infty} \sum_j \alpha_j(\tau) d\tau} \quad (7)$$

The fractional contribution of the i th mode to the total emission is given by

$$f_i = \frac{\int_0^{\infty} f_i(\tau) d\tau}{\int_0^{\infty} \sum_j f_j(\tau) d\tau} \quad (8)$$

where $f_i(\tau) = \tau \cdot \alpha_i(\tau)$. In the present paper we use only the unimodal and bimodal of Lorentzian distributions. More complex multimodal distributions (Lorentzian as well as Gaussian) are described elsewhere [45].

In the frequency domain, the measured quantities are the phase angle (ϕ_{ω}) and the demodulation factor (m_{ω}), where ω refers to the modulation frequency in rad/s. These values can be calculated from the sine (N_{ω}) and cosine (D_{ω}) transforms of the impulse response function

constructed with assumed parameter values. Using Eq. (4), these transforms are

$$N_\omega J = \int_{\tau=0}^{\infty} \frac{\alpha(\tau) \omega \tau^2}{1 + \omega^2 \tau^2} d\tau \quad (9)$$

$$D_\omega J = \int_{\tau=0}^{\infty} \frac{\alpha(\tau) \tau}{1 + \omega^2 \tau^2} d\tau \quad (10)$$

with

$$J = \int_{\tau=0}^{\infty} \alpha(\tau) \tau d\tau \quad (11)$$

For any parameter values the calculated (c) phase and modulation values are

$$\phi_{c\omega} = \arctan \left(\frac{N_\omega}{D_\omega} \right) \quad (12)$$

$$m_{c\omega} = (N_\omega^2 + D_\omega^2)^{1/2} \quad (13)$$

The parameter values $\bar{\tau}$ and $h\omega$ or α_i and τ_i are selected by comparison of the measured (ϕ_ω, m_ω) and calculated $(\phi_{c\omega}, m_{c\omega})$ values by the method of nonlinear least squares [27,47]. The goodness of fit was judged by the value of reduced χ_R^2

$$\chi_R^2 = \frac{1}{\nu} \sum_{\omega} \left(\frac{\phi_\omega - \phi_{c\omega}}{\delta\phi} \right)^2 + \frac{1}{\nu} \sum_{\omega} \left(\frac{m_\omega - m_{c\omega}}{\delta m} \right)^2 \quad (14)$$

where ν is the number of degrees of freedom, and $\delta\phi = 0.2^\circ$ and $\delta m = 0.005$, are the uncertainties in the measured phase and modulation values, respectively.

Transient Effects in Quenching

In the presence of quenching, the time decay of the fluorescence of the donor can be described by the function

$$I(t) = I_0 \exp \left[- \frac{t}{\tau_0} - C_q \int_0^t k(t') dt' \right] \quad (15)$$

where C_q denotes the bulk concentration of the quencher and $k(t)$ is the time-dependent second-order quenching rate. The $k(t)$ may be understood as being a sum of two terms: the transient term, which usually very rapidly declines with time, and a constant, time-independent term,

which describes the kinetics of quenching at very long times.

There are several models for transients in quenching [35,37,48,49]. The first model was introduced by Smoluchowski and developed by Collins and Kimball [49]. Within this model quenching may take place only when the distance between the excited donor and the quencher becomes equal to their distance of the closest approach ($r=a$). This implies the following expression for $k(t)$:

$$k(t) = 4\pi Da^2 \left[\frac{\partial y(r,t)}{\partial r} \right]_{r=a} \quad (16)$$

Here D is the mutual diffusion coefficient and function $y(r,t)$ describes the time and distance dependence of the average local concentration $C(r,t)$ of quencher in the surroundings of excited donors. The concentration $C(r,t)$ is related to $y(r,t)$ by the equation

$$C(r,t) = C_q y(r,t) \quad (17)$$

The function $y(r,t)$ satisfies the diffusion equation

$$\frac{\partial y(r,t)}{\partial t} = D \nabla^2 y(r,t) \quad (18)$$

The initial condition for $y(r,t)$ is

$$y(r,t=0) = 1 \quad (19)$$

Collins and Kimball [49] have chosen for the inner boundary condition (at $r=a$) the so-called radiation boundary condition.

$$\left[\frac{\partial y(r,t)}{\partial r} \right]_{r=a} = \frac{\kappa}{D} y(r=a,t) \quad (20)$$

where κ is the factor which indicates the flux velocity of the quenchers at the donor-quencher distance $r=a$. When κ has a finite value, this model becomes the radiation boundary condition (RBC) model of Collins and Kimball [48,49]. In the case when $\kappa \rightarrow \infty$, Eq. (20) becomes equivalent to the Smoluchowski boundary condition

$$y(r=a,t) = 0 \quad (21)$$

The outer boundary condition for the function $y(r,t)$ is

$$y(r=\infty,t) = 1 \quad (22)$$

The analytical solution of Eq. (18) with the boundary conditions (20) and (22) yields [75]

$$\int_0^t k(t') dt' = \frac{4\pi Da k_0}{4\pi Da + k_0} \left\{ t + \frac{k_0}{4\pi D^2 a \alpha^2} \left[\exp(\alpha^2 D t) \operatorname{erfc}(\alpha \sqrt{D t}) + \frac{2\alpha \sqrt{Dt}}{\sqrt{\pi}} - 1 \right] \right\} \quad (23)$$

where $k_0 = 4\pi a^2 \kappa$ and $\alpha = (4\pi Da + k_0)/(4\pi Da^2)$. (Please see the Discussion for comments on the RBC model and the results cited in Ref. 37.)

In the second model for transients in quenching, one assumes that the quenching of the excitation may occur when the electron clouds of the reacting species overlap significantly in space. The expression for the bimolecular transfer rate for energy transfer by electron exchange has been proposed by Dexter [74]. It may be written in the form

$$k(r) = k_a \exp \left[-\frac{r-a}{r_c} \right] \quad (24)$$

where a is the distance of the donor-quencher closest approach, r_c is the characteristic transfer distance, and k_a is a value of the transfer rate at $r=a$. We refer to this model as the distance-dependent quenching (DDQ) model. In the presence of material diffusion, the time-dependent transfer rate $k(t)$ is given by

$$k(t) = 4\pi \int_a^\infty r^2 k(r) y(r,t) dr \quad (25)$$

Here the function $y(r,t)$ is also governed by the diffusion equation but the equation has now an additional sink term which is responsible for the through-space fluorescence quenching,

$$\frac{\partial y(r,t)}{\partial t} = D \nabla^2 y(r,t) - k(r) y(r,t) \quad (26)$$

One assumes the initial condition and the outer boundary condition to be the same as described by Eqs. (19) and (22). At the inner boundary the former radiation boundary condition is replaced by the "reflecting" or "specular" boundary condition,

$$\left[\frac{\partial y(r,t)}{\partial t} \right]_{r=a} = 0 \quad (27)$$

This condition indicates that in the model the immediate donor-quencher encounters do not introduce any other

deactivation channel apart from that described by the rate (24). Equation (26) can be solved only numerically using the algorithm described previously [76].

Anisotropy Decays

If a sample is excited with a brief pulse of vertically polarized light, and if the fundamental anisotropy is greater than zero, the polarized excitation results in a larger population of molecules whose emission is aligned parallel to the excitation. After excitation, the initial difference between the parallel [$I_{\parallel}^Q(t)$] and perpendicular [$I_{\perp}^Q(t)$] components of the emission decays as the result of both rotational motion of the fluorophore and to decay of the total emission [$I_T^Q(t)$]. The individual polarized components decay as

$$I_{\parallel}^Q(t) = \frac{1}{3} I_T^Q(t) [1 + 2r(t)] \quad (28)$$

$$I_{\perp}^Q(t) = \frac{1}{3} I_T^Q(t) [1 - r(t)] \quad (29)$$

where the total emission is

$$I_T^Q(t) = I_{\parallel}^Q(t) + 2 I_{\perp}^Q(t) \quad (30)$$

Our approach to improving resolution is to vary the intensity decays $I_T^Q(t)$ by collisional quenching. The superscript Q indicates the quencher concentration. We assume that collisional quenching does not alter the anisotropy decay, which seems to be reasonable, as acrylamide does not appear to interact with the fluorophores or peptides [29]. Additionally, we were able to account for the data at all quencher concentrations with a single anisotropy decay law. This implies that the anisotropy decay is not altered by the quencher. The anisotropy decay law can be described as a sum of exponentials,

$$r(t) = \sum_i r_o g_i e^{-t/\theta_i} \quad (31)$$

The correlation times (θ_i) and the associated amplitudes (r_o, g_i) are determined by the size, shape, and flexibility of the molecule. For peptides the apparent correlation times are determined by the rates of rotational diffusion and by segmental motions of the fluorophore relative to the peptide.

In the frequency domain the measured quantities are the phase angle difference between the parallel and the perpendicular components of the emission ($\Delta_\omega^Q = \phi_\perp - \phi_\parallel$) and the ratio of the modulated components of the polarized emission ($\Lambda_\omega^Q = m_\parallel/m_\perp$), each measured over a range of modulation frequencies. The ani-

sotropy decay parameters are obtained by the best nonlinear least-squares fit to the data using calculated (c) values of Δ_{cw}^Q and Λ_{cw}^Q . The calculated values are obtained using

$$\Delta_{\text{cw}}^Q = \arctan \left(\frac{D_{\parallel}^Q N_{\perp}^Q - N_{\parallel}^Q D_{\perp}^Q}{N_{\perp}^Q N_{\perp} + D_{\perp}^Q D_{\perp}^Q} \right) \quad (32)$$

$$\Lambda_{\text{cw}}^Q = \left[\frac{(N_{\parallel}^Q)^2 + (D_{\parallel}^Q)^2}{(N_{\perp}^Q)^2 + (D_{\perp}^Q)^2} \right]^{1/2} \quad (33)$$

where

$$N_i^Q = \int_0^\infty I_i^Q(t) \sin \omega t dt \quad (34)$$

$$D_i^Q = \int_0^\infty I_i^Q(t) \cos \omega t dt \quad (35)$$

The goodness of fit estimated from the value of χ_R^2 is

$$\chi_R^2 = \frac{1}{v} \sum_{\omega, Q} \left(\frac{\Delta_{\omega}^Q - \Delta_{\text{cw}}^Q}{\delta \Delta} \right)^2 + \frac{1}{v} \sum_{\omega, Q} \left(\frac{\Lambda_{\omega}^Q - \Lambda_{\text{cw}}^Q}{\delta \Lambda} \right)^2 \quad (36)$$

where $\delta \Delta$ and $\delta \Lambda$ are the uncertainties in the phase angle and modulation ratio (0.1° and 0.005), respectively. The data obtained for several quencher concentrations were analyzed simultaneously to obtain the anisotropy decay [Eq. (21)]. The Λ_{ω} ratios are presented in an alternative form [50,51], as the frequency-dependent modulated anisotropy

$$r_{\omega} = \frac{\Lambda_{\omega} - 1}{\Lambda_{\omega} + 2} \quad (37)$$

The values of r_{ω} are comparable to those of the steady-state anisotropy (r) and the fundamental anisotropy (r_o). At low modulation frequencies, r_{ω} is nearly equal to r . At high modulation frequencies, r_{ω} approaches r_o .

MATERIALS AND METHODS

Frequency-domain data were obtained on the instrument with an upper frequency limit of 2 GHz [23]. The excitation source was the 3.795-MHz cavity-dumped output from a Coherent Model 700 dye laser with the dye rhodamine 6G. The second jet was used with the saturable absorber DODCI (3,3'-diethyl-2,2'-oxadicarbocyanine iodide). The dye laser was synchronously pumped at 76 MHz using a mode-locked argon ion laser, Coherent Innova 15, about 900 mW at 514 nm, with a pulse width of 5 ps. The visible cavity-dumped output

of the dye laser was typically near 80 mW. To obtain 287 nm for excitation of tyrosine we used a Spectra Physics Model 390 frequency doubler, with a KDP angle tuned crystal.

NATyrA was obtained from Aldrich. Oxytocin and lysine-vasopressin were from Sigma. We found oxytocin to be 98% pure, and vasopressin to be 99.5% pure, by HPLC in acetonitrile/water with 0.1% trifluoroacetic acid as the mobile phase. Their emission spectra were characteristic of tyrosine. Acrylamide was from BioRad, electrophoresis grade, 99.9% pure.

The experiments were performed in 0.05 M phosphate (pH 7.0) at 25°C. The emission was observed through an interference filter with a maximum of transmittance at 302 nm (10-nm bandpass). Examination of buffer with acrylamide (if used) indicated that background fluorescence and/or scattered light contributed less than 1% to the measured emission.

RESULTS

Lifetime Analysis

Frequency-domain intensity data are shown for vasopressin in Fig. 1. To observe the complete frequency

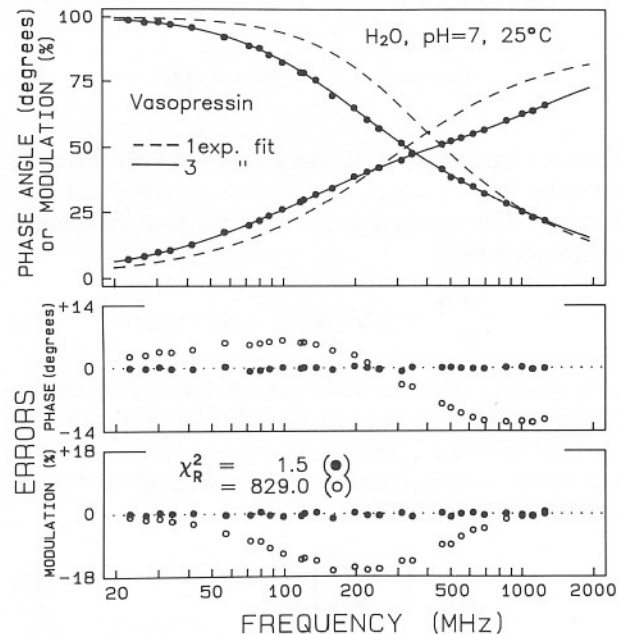


Fig. 1. Phase and modulation data for vasopressin tyrosine fluorescence intensity decay. The dashed line is the best single-exponential fit, and the solid line is the best three-exponential fit.

response of the emission it was necessary to use modulation frequencies as high as 1.3 GHz. The dashed line shows the best fit to a single-exponential decay, which is obviously inadequate to account for the data. The double-exponential model is also inadequate, as can be seen from the relative value of χ_R^2 (Table I). Three decay times were needed to account for the data, resulting in a fourfold decrease in χ_R^2 as compared to the double-exponential fit (Table I). It is probable that the decay times have their origin in distinct conformation states, i.e., rotomer model, as described by Ross *et al.* for oxytocin [4] and several laboratories for tryptophan [52–54].

The intensity decay of oxytocin was also found to be complex, requiring three decay times to account for the data. The mean decay time of oxytocin is 0.75 ns, which is about 20% smaller than that of vasopressin. It is interesting to note that the intensity decay of NATyrA itself was somewhat heterogeneous and required two decay times to account for the data. Evidently, some quenching process is present in the peptides, which shortens their decay times relative to that of NATyrA, 1.5 ns. Heterogeneous intensity decays for tyrosine and tyrosyl peptides have been observed previously [12, 55–57].

We also analyzed the intensity decays using the uni- and bimodal Lorentzian distribution models. This seems reasonable in that one might expect a range of solution conformations, each of which could display somewhat different decay kinetics. We found that the goodness of fit obtained for bimodal Lorentzian distribution were the same as those for the three-component multiexponential analyses. This is not surprising because in both models the same number of floating parameters (five) is used. Consequently, a selection between these models must be based on criteria other than statistical considerations. The lifetime distributions can be considered an alternative presentation of the intensity decay data.

The lifetime distributions obtained for the three tyrosine compounds are shown in Fig. 2. A narrow bimodal distribution was seen for NATyrA, suggesting the presence of two dominant emitting species and/or dynamic averaging of the conformation during the lifetime of the excited state. Wider distributions were found for the peptides. The shorter lifetime in the vasopressin has a higher amplitude and is much more narrow than for oxytocin. In contrast, the longer lifetime for vasopressin has a lower amplitude but more width than for oxytocin. One possible origin for the lifetime distribution is the range of conformation states available to these molecules and the different surroundings of the tyrosyl residue for oxytocin and vasopressin.

Table I. Multiexponential Analysis of Tyrosyl Fluorescence Intensity Decays in 50 mM Phosphate, pH 7, at 25°C

Acrylamide	τ_i (ns)	$\bar{\tau}$ (ns)	α_i	f_i	χ_R^2 (1/2) ^a
NATyrA					
0 M	1.42		1	1	73.0
	0.20		0.210	0.032	
	1.55	1.51	0.790	0.968	2.3
0.1 M	0.69		1	1	195.5
	0.16		0.349	0.091	
	0.85	0.79	0.651	0.902	1.8
0.2 M	0.42		1	1	282.8
	0.12		0.453	0.145	
	0.58	0.51	0.547	0.855	2.0
0.3 M	0.33		1	1	385.6
	0.04		0.531	0.100	
	0.44	0.40	0.469	0.900	3.4
Oxytocin					
0 M	0.63		1	1	374.4/5.9
	0.08		0.292	0.045	
	0.36		0.275	0.189	
	0.93	0.78	0.433	0.766	2.1
0.1 M	0.45		1	1	799.2/4.8
	0.06		0.536	0.103	
	0.32		0.221	0.229	
	0.84	0.64	0.242	0.667	1.4
0.2 M	0.30		1	1	732.9/7.1
	0.04		0.593	0.131	
	0.28		0.274	0.389	
	0.72	0.46	0.133	0.480	1.6
0.3 M	0.24		1	1	614.3/6.4
	0.03		0.682	0.159	
	0.30		0.260	0.552	
	0.68	0.37	0.058	0.289	1.8
Vasopressin					
0 M	0.59		1	1	829.0/5.5
	0.17		0.592	0.205	
	0.75		0.301	0.452	
	1.60	0.92	0.107	0.343	1.5
0.1 M	0.40		1	1	549.4/2.9
	0.08		0.567	0.150	
	0.55		0.420	0.783	
	1.49	0.54	0.013	0.067	1.2
0.2 M	0.30		1	1	469.3/2.3
	0.04		0.577	0.123	
	0.41		0.416	0.832	
	1.30	0.40	0.007	0.045	0.8
0.3 M	0.23		1	1	516.3/3.3
	0.03		0.684	0.152	
	0.32		0.308	0.783	
	1.00	0.32	0.008	0.064	0.9

^a Where shown, the second number is the value of χ_R^2 from the two-exponential fit.

We questioned whether the lifetime distributions shown in Fig. 2 were statistically different. Hence, we attempted to fit the data for one peptide with the lifetime distribution parameters found for the other peptide (Ta-

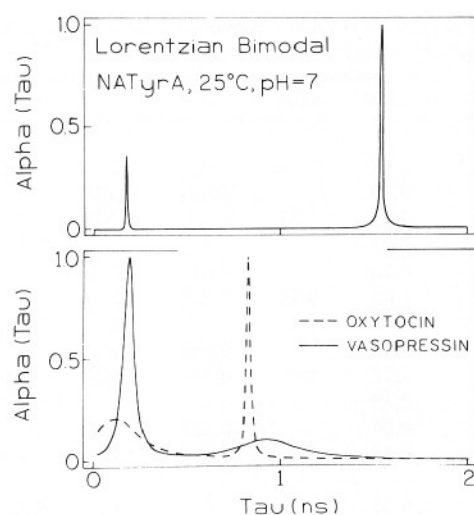


Fig. 2. Lorentzian bimodal lifetime distributions. Top, NATyrA; bottom, oxytocin (dashed line) and vasopressin (solid line).

Table II. Lifetime Distribution Analysis of Tyrosyl Fluorescence Using Lorentzian Uni- and Bimodal Models

Compound	$\bar{\tau}$ (ns)	hw (ns)	g_i	χ_R^2
NATyrA	1.31	1.003	1	20.6
	0.18	0.002	0.204	
	1.54	0.060	0.796	2.5
Oxytocin	0.25	0.877	1	30.8
	0.06	0.329	0.760	
	0.83	0.020	0.240	2.1
	<0.061>	<0.627>		
Vasopressin	<0.371>	<0.373>		71.1
	0.10	0.584	1	15.6
	0.18	0.061	0.627	
	0.93	0.371	0.373	1.5
	<0.329> ^a	<0.760>		
	<0.020>	<0.240>		78.0

^a These parameters were held fixed at the values found for oxytocin.

ble II). This resulted in an unacceptable value of $\chi_R^2 = 78$ or 71, which in turn suggests that the lifetime distributions for oxytocin and vasopressin are distinct. While not presented in the present report, it should be possible to correlate these distributions with the local environment around the tyrosine residues.

Fluorescence Quenching

Acrylamide is known to be a quencher of protein fluorescence, especially for tryptophan-containing pro-

teins [30,31,58,59]. Acrylamide is also an effective quencher of tyrosine fluorescence. Since we were interested in interpreting the quenching data in terms of fluorophore-quencher contact, we first evaluated the possibility of nonradiative energy transfer [60] between tyrosine (donor) and acrylamide (acceptor). We found the Forster distance (R_o) for this donor-acceptor system to be 3.6 Å, which is nearly two times smaller than the interaction radius of 7 Å for quenching. Hence, the quenching of tyrosine due to energy transfer is negligible, and in any event, molecular contact seems to be required for quenching.

The parameters recovered from multiexponential analysis of quenched samples are shown in Table I. It is known that, with quenching, homogeneous decays generally become more heterogeneous. This effect is easily seen for NATyrA, where the values of χ_R^2 increase several-fold with quenching. The increased heterogeneity due to quenching is also seen for oxytocin, where values of χ_R^2 for the single-exponential fit increase about twofold. However, the intensity decay of vasopressin is already strongly heterogeneous, and the effect of quenching was not evident in any further increase in χ_R^2 (Table I).

We used the mean decay times calculated from Table I to construct Stern-Volmer plots (Fig. 3). It is evident that oxytocin is much less quenched than vasopressin (the ratio of Stern-Volmer constants equals 1.8). For

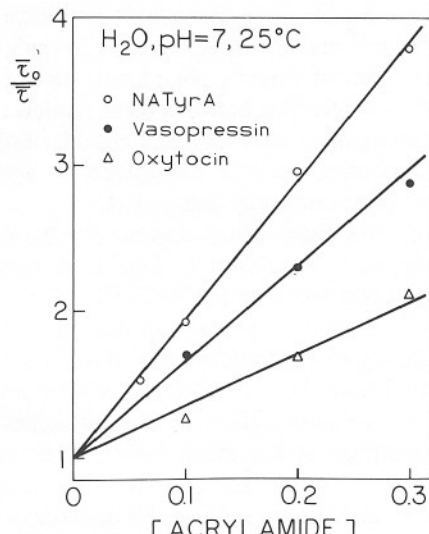


Fig. 3. Stern-Volmer plot for acrylamide quenching of NATyrA (○), vasopressin (●), and oxytocin (△). The mean decay times in the absence of acrylamide, given by $\bar{\tau} = \sum f_i \tau_i$, are 1.51, 0.78, and 0.92 ns for NATyrA, oxytocin, and vasopressin, respectively.

NATyrA we obtained $K_{sv} \sim = 10 M^{-1}$, which is less than obtained from steady-state intensity measurements by [34] ($K_{sv} = 14 M^{-1}$). We suspect that the difference in these results is due to the strong inner filter effects of acrylamide at 285 nm and that it would be difficult to recover correct parameters of quenching from steady-state intensity measurements even using careful procedures. It is probable that the decay time measurements, which are insensitive to inner filter effects, yield more reliable quenching constants. However, it should also be noted that the time-resolved measurements do not detect the presence of dark complexes, i.e., static quenching, which is detected by decreased intensity in the steady-state measurements.

We used the RBC and DDQ models for transient effects in quenching to evaluate the frequency-domain data for the quenched samples. In general, we found that the data were less well fit to the RBC model than to the DDQ model. Hence, parameter values are only reported for the DDQ analysis. Frequency-domain data for NATyrA and for the two peptides are shown in Figs. 4–6. The solid lines show the best fit to the data using the DDQ model and global analysis at three quencher concentrations. The dashed lines show the best fit to the radiation model and are shown only where significantly different from the DDQ model. The results of the individual and the global analyses are summarized in Table III. In all these analyses, the encounter radius was held fixed at 7 Å, and for the DDQ model the interaction distance (r_e) was held fixed at 0.7 Å. In our opinion the most reliable parameters are obtained from simultaneous analysis with acrylamide concentrations of 0–0.3 M. We note that improved values of χ_R^2 were found for the DDQ model, which suggests the presence of a distance-dependent rate constant for quenching. This conclusion is most strongly

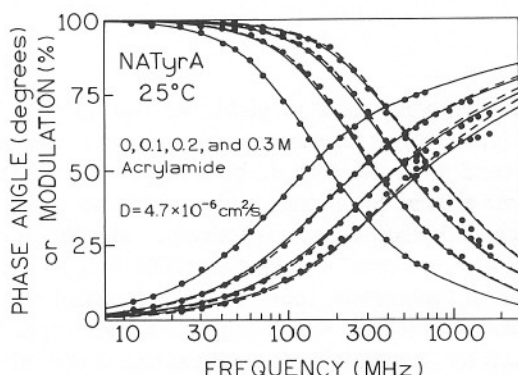


Fig. 4. Global fit to DDQ model for NATyrA quenched by acrylamide. The dashed lines show the best global fit to the radiation model.

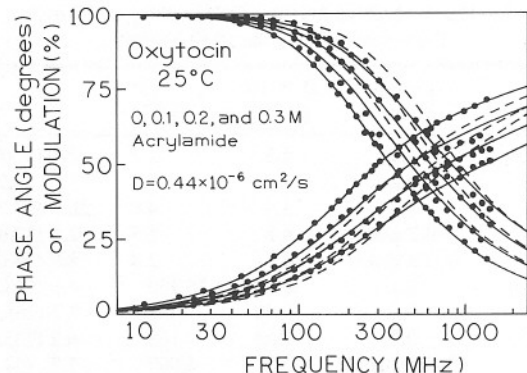


Fig. 5. Global fit to DDQ model for oxytocin quenched by acrylamide. The dashed lines show the best global fit to the radiation model.

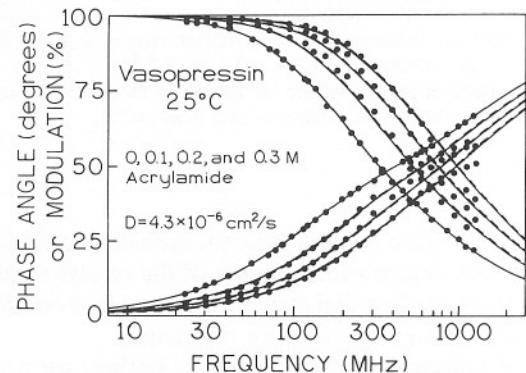


Fig. 6. Global fit to DDQ model for vasopressin quenched by acrylamide. The dashed lines show the best fit to the radiation model.

indicated for acrylamide quenching of oxytocin, but this conclusion requires further validation prior to claiming that a definitive observation of such a quenching mechanism. However, we have also observed a distance-dependent quenching rate for 1,2-benzanthracene by CBr₄ [77].

The diffusion coefficient recovered for acrylamide quenching of NATyrA ($D = 4.7 \times 10^{-6} \text{ cm}^2/\text{s}$ and $\kappa = 205 \text{ cm/s}$) can be compared to that obtained previously for *N*-acetyl-*L*-tryptophamide ($2.1 \times 10^{-5} \text{ cm}^2/\text{s}$) [42]. The discrepancy between the diffusion coefficients may be the result of a flaw in our earlier algorithm [37] (see Comment at the end of the Discussion). The diffusion coefficients obtained for oxytocin and vasopressin show dramatic differences (0.44×10^{-6} and $4.3 \times 10^{-6} \text{ cm}^2/\text{s}$ for oxytocin and vasopressin, respectively). These results suggest that the acrylamide molecules can reach tyrosine in vasopressin much easier than in oxy-

Table III. Analysis of Acrylamide Quenching of Tyrosyl Fluorescence Using the DDQ Model^a

Compound	[Acrylamide]	$D \times 10^6$ (cm ² /s)	$k_a \times 10^{-11}$ (s ⁻¹)	χ_R^2
NATyrA	0.1	5.3	2.1	2.1 (5.5) ^b
	0.2	4.5	4.2	1.6 (19.9)
	0.3	3.4	4.8	26.7 (67.2)
	0–0.2 global	4.8	3.3	2.1 (10.0)
	0–0.3 global	4.6	2.4	18.8 (29.0)
	Oxytocin	0.1	26,700	4.5 (138.3)
Oxytocin	0.2	0.40	1,490	2.1 (151.5)
	0.3	0.68	165	6.2 (135.8)
	0–0.2 global	0.21	4,000	7.7 (94.5)
	0–0.3 global	0.44	602	15.0 (104.0)
	Vasopressin	0.1	12.4	0.23
Vasopressin	0.2	8.6	0.25	27.7 (27.5)
	0.3	2.9	1.6	21.2 (29.5)
	0–0.2 global	10.5	0.24	16.1 (16.0)
	0–0.3 global	4.3	0.54	21.9 (21.5)

^a The interaction radius (a) and the interaction distance (r_e) were held fixed for all analyses at $a = 7 \text{ \AA}$ and $r_e = 0.7 \text{ \AA}$.

^b The numbers in parentheses are the χ_R^2 values for the RBC model, in which the interaction radius was held fixed at 7 Å.

tocin. We believe that the apparent diffusion coefficient reflects that degree with exposure of the tyrosyl residue to the aqueous phase and that this exposure is severalfold higher for vasopressin than for oxytocin.

To substantiate this observation further, we questioned the uncertainties in the diffusion coefficients recovered from the DDQ model. To accomplish this we examined the values of χ_R^2 when D was held constant while k_a was variable. The least-squares analysis was performed again, allowing the floating parameter to vary, yielding the minimum value of χ_R^2 consistent with the fixed D . This procedure should account for the correlation between D and k_a and, also, demonstrated that we were not in a local minimum for the oxytocin analysis. These χ_R^2 surfaces are shown in Fig. 7. These results demonstrate that the apparent diffusion coefficients for acrylamide quenching are unique and nonoverlapping for oxytocin and vasopressin.

Anisotropy Decays

Anisotropy decay data were measured and analyzed globally using progressively quenched samples (Figs. 8–10). Parameters recovered from the global analysis are summarized in Table IV. The limiting anisotropies recovered from the analysis are in good agreement with measured values at -60°C in propylene glycol [61]. For NATyrA we recovered only one correlation time of 42

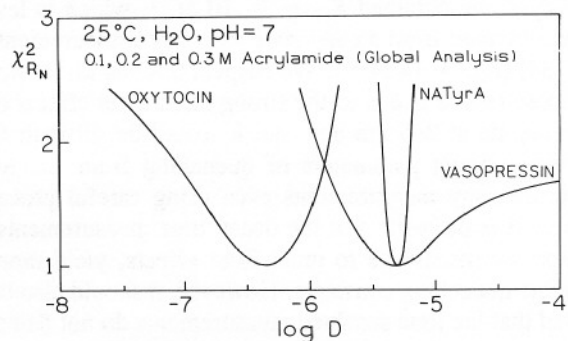


Fig. 7. χ_R^2 surfaces for diffusion coefficients recovered from radiation model for acrylamide quenching of NATyrA, oxytocin, and vasopressin.

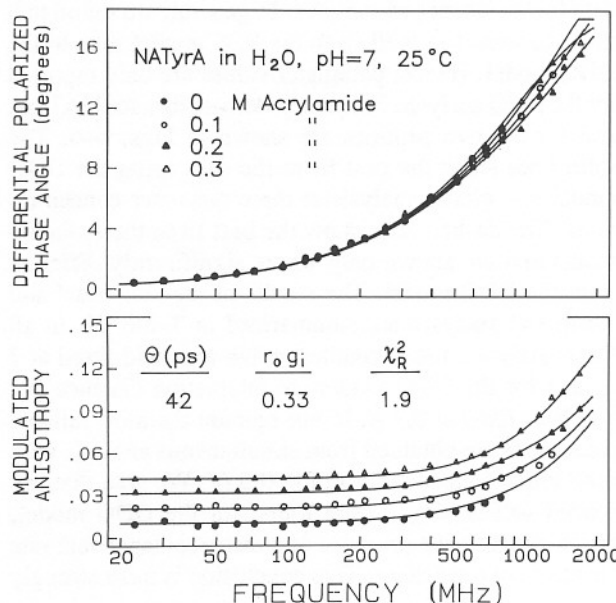


Fig. 8. Differential phase and modulation anisotropy data for NATyrA quenched by acrylamide (global fit with four acrylamide concentrations).

ps (the two-component fit yields 42 and 43 ps). For oxytocin, as well as for vasopressin, two correlation times are needed to fit the data. In both cases we get nearly the same shorter correlations times of 34 and 37 ps for oxytocin and vasopressin, respectively, and a 100-ps difference in longer correlation time near 500–600 ps. Overall rotation of vasopressin appears to be somewhat slower than that of oxytocin, which suggests a more expanded structure for vasopressin. A more expanded structure is expected to display slower overall rotational diffusion. Importantly, the amplitude of the faster picosecond com-

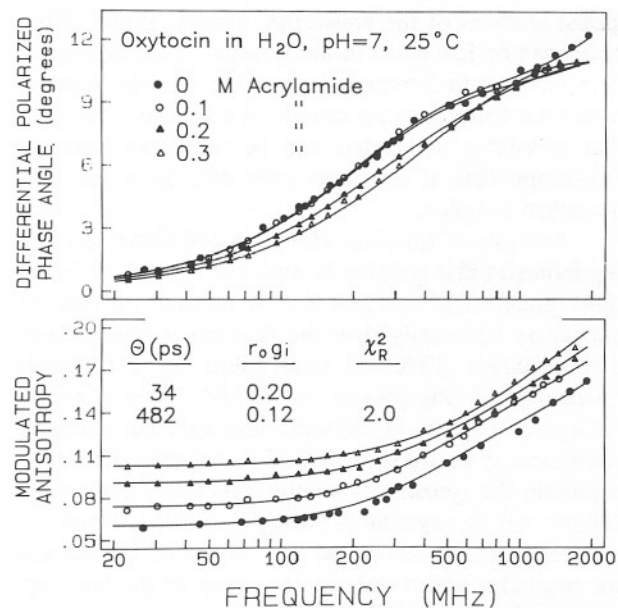


Fig. 9. Differential phase and modulated anisotropy data for oxytocin quenched by acrylamide. The solid lines represent the global fit with four acrylamide concentrations.

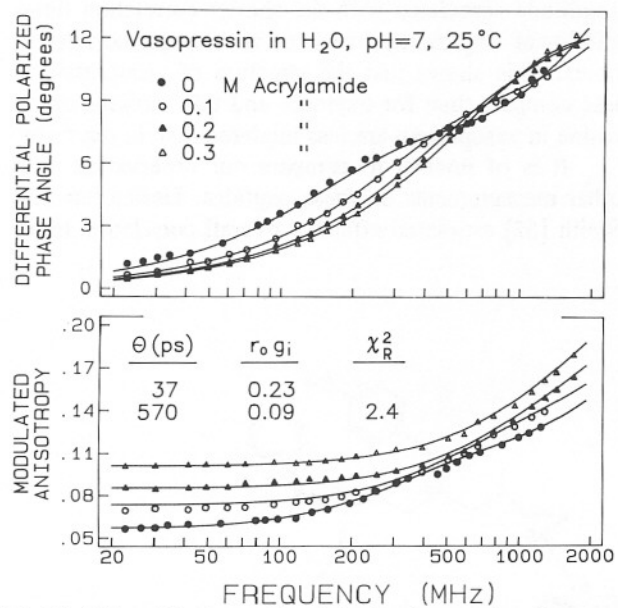


Fig. 10. Differential phase and modulated anisotropy data for vasopressin quenched by acrylamide. The solid lines represent the global fit for four acrylamide concentrations.

ponent is larger for vasopressin than for oxytocin. For these peptides 62 and 72%, respectively, of the aniso-

Table IV. Global Analysis (0, 0.1, 0.2, and 0.3 M Acrylamide) of Tyrosyl Anisotropy Decays in 50 mM Phosphate, pH 7, at 25°C

	θ_i (ps)	$r_0 g_i$	χ^2_R
NATyrA	42	0.33	1.9
	42	0.20	—
	43	0.12	1.9
	193	0.22	76.2
Oxytocin	34	0.20	—
	482	0.12	2.0
	54	<0.23>	—
	447	<0.09>	95.9
Vasopressin	175	0.21	75.5
	37	0.23	—
	570	0.09	2.4
	26	<0.20>	—
	591	<0.12>	68.5

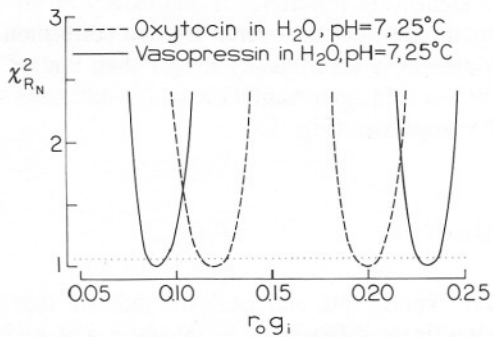


Fig. 11. χ^2 surfaces for amplitudes $r_0 g_i$ recovered from global analysis of anisotropy decays.

tropy decays via the segmented motions. This result also suggests a more flexible solution structure for vasopressin than for oxytocin.

We questioned whether the differences in the anisotropy decays were statistically significant. We attempted to fit the anisotropy data for each peptide to the best fit anisotropy parameters for the other peptide. This resulted in unacceptable elevations in χ^2_R (Table IV). Next we examined the χ^2 surface both for the amplitude of the anisotropy decays (Fig. 11) and for the correlation times (Fig. 12). Examination of the χ^2 surfaces indicates that it is difficult to recover these parameters from measurements using only nonquenched samples (not shown). However, it is evident from the global analysis that the difference in amplitudes is significant with our experimental data. The lower amplitudes for the shorter and higher amplitudes for longer correlation times in oxytocin anisotropy decay means that tyrosine has less

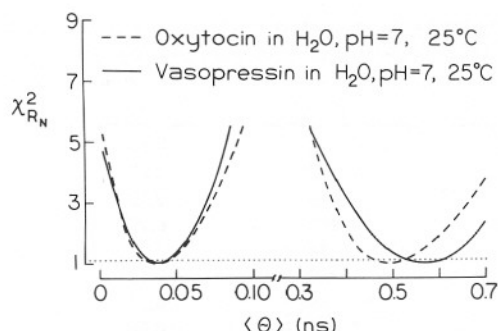


Fig. 12. χ^2_{RN} surfaces for the correlation times recovered from the global anisotropy analysis.

freedom in oxytocin than in vasopressin and that oxytocin has more compact structure than vasopressin. There was no significant difference in the values of the short correlation times, but the overall rotation correlation time of vasopressin is significantly longer than that of oxytocin, which is in agreement with a more extended structure of vasopressin (Fig. 13).

DISCUSSION

Our experiments and analyses indicate that there exist significant differences in dynamic and hydrodynamic properties of oxytocin and vasopressin. These differences were most evident when experimental data were analyzed by nontraditional methods, i.e., lifetime distributions, transient effects in collisional quenching, and

global analysis of the anisotropy decays. While differences can be identified in the tyrosine intensity decays, it is difficult to interpret these parameters in terms of molecular features of the sample. It should also be noted that unreliable parameters can be recovered from the anisotropy data if one uses only data from the non-quenched samples.

Analysis of transient effects in collisional quenching indicates that tyrosine in oxytocin is shielded by the other amino acid residues and is reached by external quenchers less easily than the tyrosine in vasopressin. The apparent diffusion coefficient for acrylamide quenching of vasopressin is 10-fold lower than for NATyrA, whereas in oxytocin this apparent diffusion coefficient is nearly identical. This suggests that in vasopressin the tyrosine is nearly completely exposed to solvent and in oxytocin is strongly shielded. However, we feel uncertain about the low values of D observed for oxytocin, which may be the result of the large apparent values of k_a (Table III). At this time we do not understand the factors which influence the values of k_a .

Global analysis of the anisotropy decay data indicates that, in contrast to NATyrA, a single-exponential model is not adequate to account for the anisotropy decay of oxytocin and vasopressin. Vasopressin has a higher amplitude associated with the shorter correlation times and lower amplitudes associated with longer correlation times. This shows that the structure of vasopressin is less compact than for oxytocin and that motions of tyrosine in vasopressin are less hindered than in oxytocin.

It is of interest to compare our observation with other measurements on these peptides. Deslauriers and Smith [62] estimated effective overall correlation times

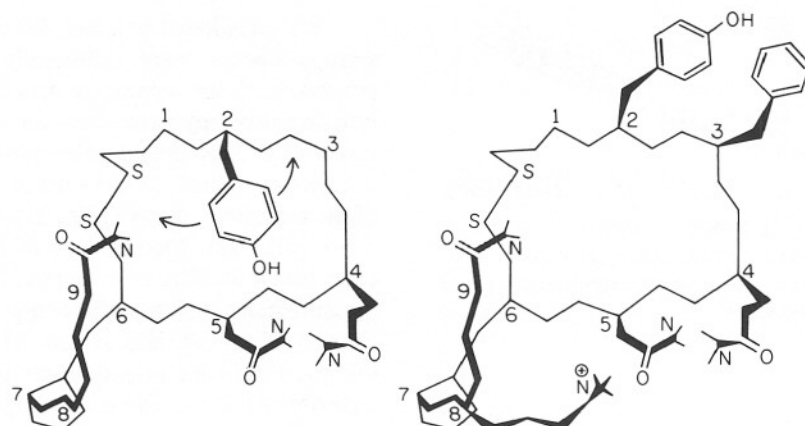


Fig. 13. Structures of oxytocin (left) and vasopressin (right) consistent with our results.

(from ^{13}C spin-lattice relaxation study) for both hormones. These results, ~ 0.5 ns, are in satisfactory agreement with our longer correlation times, which we assign to overall rotational diffusion. Paladini and co-workers performed dialysis studies for oxytocin and vasopressin using a thin-film technique [5]. Their results indicate that oxytocin has a compact conformation with tripeptide tail held close to the ring, whereas vasopressin has a more extended conformation because of the repulsion between the basic groups in the ring and the tail. In a series of elegant papers beginning in 1971 (based mostly on NMR and CD measurements), Urry, Walter and collaborators, and Hruby and co-workers, synthesized biologically active models for oxytocin and vasopressin [63–71]. One of the most important differences between these models (Fig. 13) is that, in oxytocin, the tyrosine is located in a hydrophylic cleft (present in the models of both hormones), and in vasopressin, the tyrosine is located out of this cleft and the aromatic ring is in a stacking interaction with phenylalanine [9,62,68,72]. Recent studies of the emission from ionized tyrosine (tyrosinate) yield a similar conclusion [73]. Our results are generally in agreement with these experiments and models for the hormones. However, our quenching and anisotropy results show that it is unlikely that stacking interactions between tyrosine-phenylalanine aromatic rings of vasopressin are static, in that the vasopressin tyrosine is mobile and accessible to acrylamide on the subnanosecond time scale. If these interactions were static on this time scale, then this interaction should shield fluorophore from quencher and hinder tyrosine local motions.

Recent articles about theoretical calculations of conformations and molecular dynamics of oxytocin and vasopressin [1,6] have indicated several possible conformations and a high flexibility for both hormones. It should be noted that the molecular dynamics calculation on vasopressin [1] indicates that the tyrosyl and phenylalanyl residues were not always in stacked and/or adjacent configurations, which is in agreement with the high dynamic accessibility which we found for the tyrosyl residues. In total, the theoretical calculations on these peptides are in agreement with our results, explain the fast and slow components which we found in anisotropy decays, and are consistent with the dynamic accessibility of the tyrosyl residues to quenchers.

Comment on the RBC Model

We wish to comment on a possible error in our earlier report on the RBC model [37]. In that paper we indicated that iodide and acrylamide quenching of indole was well described by the RBC model. It now appears

that our algorithm was flawed in a manner which mimicked the DDQ model which fits the data and that the data are not consistent with the RBC model. This issue is now being investigated and is mentioned here to alert other laboratories to this possible error.

ACKNOWLEDGMENTS

This work was supported by Grants GM-39617 from the National Institutes of Health and DMB-8804931 from the National Science Foundation. Support for frequency domain instrumentation was provided by the National Science Foundation, Grants DIR-8710401 and DMB-8502835, and by the National Institutes of Health, Grant RR-04800. This work was supported in part by the Medical Biotechnology Center at the University of Maryland.

REFERENCES

1. A. T. Hagler, D. J. Osguthorpe, P. Dauber-Osguthorpe, and J. C. Hempel, (1985) *Science* **227**, 1309–1315.
2. D. H. Live, H. R. Wyssbrod, A. J. Fischman, W. C. Agosta, C. H. Bradley, and D. Cowburn (1979) *J. Am. Chem. Soc.* **101**, 474–479.
3. J. A. Glasel, V. J. Hruby, J. F. McKelvy, and A. F. Spatola (1973) *J. Mol. Biol.* **79**, 555–575.
4. J. B. A. Ross, W. R. Laws, A. Buku, J. C. Sutherland, and H. R. Wyssbrod (1986) *Biochemistry* **25**, 607–612.
5. L. C. Craig, E. J. Harfenist, and A. C. Paladini (1964) *Biochemistry* **3**, 764–769.
6. J. R. Somoa and J. W. Brady (1988) *Biopolymers* **27**, 939–956.
7. S. P. Wood, I. J. Tickle, A. M. Trebarne, J. E. Pitts, Y. Masa-crenhas, J. Y. Li, J. Husain, S. Cooper, T. L. Blundell, V. Hruby, A. Buku, A. J. Fischman, and H. R. Wyssbrod (1986) *Science* **232**, 633–636.
8. D. A. Langs, G. D. Smith, J. J. Stezowski, and R. E. Huges (1986) *Science* **232**, 1240–1242.
9. C. W. Smith (1981) in D. H. Schlesinger (Ed.), *Neurohypophyseal Peptide Hormones and Other Biological Active Peptides*, Elsevier North-Holland, Amsterdam, pp. 23–25.
10. J. B. A. Ross, W. R. Laws, K. W. Rousslang, and H. R. Wyssbrod (1992) in J. R. Lakowicz (Ed.), *Fluorescence Spectroscopy, Vol 3. Biochemical Applications*, Plenum, New York (in press).
11. J. B. A. Ross, W. R. Laws, J. C. Sutherland, A. Buku, P. G. Katsoyannis, I. L. Schwartz, and H. R. Wyssbrod (1986) *Photochem. Photobiol.* **44**, 365–370.
12. J. R. Lakowicz, G. Laczko, and I. Gryczynski (1987) *Biochemistry* **26**, 82–90.
13. I. Yamazaki, N. Tamai, H. Kume, H. Tsuchiya, and K. Oba (1985) *Rev. Sci. Instrum.* **56**, 1187–1194.
14. E. W. Small, L. J. Libertini, and I. Isenberg (1984) *Rev. Sci. Instrum.* **55**, 879–885.
15. A. van Hoek, J. Vervoost, and A. J. W. G. Visser (1983) *J. Biochem. Biophys. Methods* **7**, 243–254.
16. D. J. S. Birch, A. S. Holmes, J. R. Gilchrist, R. E. Imhof, S. M. Al-Shawi, and B. Nadolski (1987) *J. Phys. E. Sci. Instrum.* **20**, 471–473.
17. D. V. O'Conner and D. Phillips (1984) *Time-Correlated Single Photon Counting*, Academic Press, New York.
18. A. J. W. G. Visser (Ed.), (1985) *Anal. Instrum.* **14**, 193–566.

19. J. R. Lakowicz, M. L. Johnson, I. Gryczynski, H. Szmacinski, N. Joshi, and G. Laczko (1988) *SPIE* **909**, 170–177.
20. J. R. Lakowicz (Ed.) (1990) *SPIE* **1204**, 1–850.
21. E. Gratton and M. Limkeman (1983) *Biophys. J.* **44**, 315–323.
22. J. R. Lakowicz and B. P. Maliwal (1985) *Biophys. Chem.* **21**, 61–73.
23. J. R. Lakowicz, G. Laczko, and I. Gryczynski (1986) *Rev. Sci. Instrum.* **57**, 2499–2506.
24. G. Laczko, I. Gryczynski, Z. Gryczynski, W. Wiczka, H. Malak, and J. R. Lakowicz (1990) *Rev. Sci. Instrum.* **61**, 2331–2337.
25. J. M. Beechem, J. R. Knutson, J. A. B. Ross, B. J. Turner, and L. Brand (1983) *Biochemistry* **22**, 6054–6063.
26. J. R. Knutson, J. M. Beechem, and L. Brand (1983) *Chem. Phys. Lett.* **102**, 501–507.
27. J. R. Lakowicz, E. Gratton, G. Laczko, H. Cherek, and M. Limkeman (1984) *Biophys. J.* **46**, 463–477.
28. J. R. Lakowicz, H. Cherek, I. Gryczynski, N. Joshi, and M. L. Johnson (1987) *Biophys. J.* **51**, 755–768.
29. M. R. Eftink and C. A. Ghiron (1987) *Biochim. Biophys. Acta* **916**, 343–349.
30. M. R. Eftink and C. A. Ghiron (1981) *Anal. Biochem.* **114**, 199–227.
31. J. R. Lakowicz, *Principles of Fluorescence Spectroscopy*, Plenum Press, New York, 1983.
32. H. C. E. M. Marsch, G. K. A. Kochler, and R. G. Hiskey (1981) *Biochim. Biophys. Acta* **667**, 35–42.
33. M. C. Cubbin and C. M. Kay (1980) *FEBS Lett.* **22**, 72–76.
34. A. Follenius and D. Gerard (1983) *Photochem. Photobiol.* **38**, 373–378.
35. N. Joshi, M. L. Johnson, I. Gryczynski, and J. R. Lakowicz (1987) *Chem. Phys. Lett.* **135**, 200–207.
36. J. R. Lakowicz, M. L. Johnson, N. Joshi, I. Gryczynski, and G. Laczko (1986) *Chem. Phys. Lett.* **131**, 343–348.
37. J. R. Lakowicz, M. L. Johnson, I. Gryczynski, N. Joshi, and G. Laczko (1987) *J. Phys. Chem.* **91**, 3277–3285.
38. J. M. G. Martinho and M. A. Winnik (1987) *J. Phys. Chem.* **91**, 3640–3644.
39. D. J. S. Birch, A. D. Dutch, R. E. Imhof, B. Z. Nadolski, and I. Soutar (1987) *J. Photochem.* **38**, 239–254.
40. W. R. Ware and T. L. Nemzek (1973) *Chem. Phys. Lett.* **23**, 557–563.
41. T. L. Nemzek and W. R. Ware (1975) *J. Chem. Phys.* **62**, 447–453.
42. J. R. Lakowicz, N. B. Joshi, M. L. Johnson, H. Szmacinski, and I. Gryczynski (1987) *J. Biol. Chem.* **262**, 10907–10910.
43. J. R. Alcalá, E. Gratton, and F. G. Prendergast (1987) *Biophys. J.* **51**, 587–596.
44. J. R. Alcalá, E. Gratton, and F. G. Prendergast (1987) *Biophys. J.* **51**, 925–936.
45. J. R. Lakowicz, H. Cherek, I. Gryczynski, N. Joshi, and M. L. Johnson (1987) *Biophys. Chem.* **28**, 35–50.
46. I. Gryczynski, J. R. Lakowicz, and M. Eftink (1988) *Biochim. Biophys. Acta* **954**, 244–252.
47. E. Gratton, J. R. Lakowicz, B. P. Maliwal, H. Cherek, and M. Limkeman (1984) *Biophys. J.* **46**, 473–486.
48. F. C. Collins (1950) *J. Colloid Sci.* **5**, 499–505.
49. F. C. Collins and G. E. Kimball (1949) *J. Colloid Sci.* **4**, 425–437.
50. B. P. Maliwal and J. R. Lakowicz (1986) *Biochim. Biophys. Acta* **873**, 161–169.
51. B. P. Maliwal and J. R. Lakowicz (1986) *Biochim. Biophys. Acta* **873**, 161–172.
52. A. G. Szabo and D. M. Rayner (1980) *J. Am. Chem. Soc.* **102**, 554–563.
53. B. Donzel, J. P. Gauduchon, and Ph. Wahl (1974) *J. Am. Chem. Soc.* **96**, 801–808.
54. R. J. Robbins, G. R. Fleming, G. S. Beddard, G. Robinson, P. J. Thistlethwaite, and G. J. Woolfe (1980) *J. Am. Chem. Soc.* **102**, 6271–6279.
55. W. R. Laws, J. B. A. Ross, H. R. Wyssbrod, J. M. Beechem, L. Brand, and J. C. Sutherland (1986) *Biochemistry* **25**, 599–607.
56. J. R. Lakowicz, G. Laczko, and I. Gryczynski (1986) *Biophys. Chem.* **24**, 97–100.
57. I. Gryczynski, J. R. Lakowicz, and R. F. Steiner (1988) *Biophys. Chem.* **30**, 49–59.
58. M. R. Eftink and C. A. Ghiron (1976) *J. Phys. Chem.* **80**, 486–493.
59. M. R. Eftink and C. A. Ghiron (1977) *Biochemistry* **16**, 5546–5551.
60. T. Forster (1948) *Annal. Phys. Ser. 6* **2**, 55–75.
61. J. R. Lakowicz and I. Gryczynski (1990) unpublished observation.
62. R. Deslauriers and I. C. P. Smith (1970) *Biochem. Biophys. Res. Commun.* **40**, 179–185.
63. D. W. Urry and R. Walter (1971) *Proc. Natl. Acad. Sci. USA* **68**, 956–958.
64. R. Walter, J. D. Glickson, I. L. Schwartz, R. T. Havran, J. Meinhofer, and D. W. Urry (1972) *Proc. Natl. Acad. Sci. USA* **69**, 1920–1924.
65. J. D. Glickson, D. W. Urry, and R. Walter (1972) *Proc. Natl. Acad. Sci. USA* **69**, 2566–2569.
66. R. Walter (1972) in H. Hansen and H. Takubke (Eds.), *Peptides*, North-Holland, Amsterdam, pp. 324–327.
67. R. Deslauriers, I. C. P. Smith, and R. Walter (1974) *J. Am. Chem. Soc.* **96**, 2289–2291.
68. R. Walter (1977) *Fed. Proc.* **36**, 1872–1878.
69. V. J. Hruby (1980) in B. Weinstein (Ed.), *Chemistry and Biochemistry of Amino Acids, Peptides and Proteins*, Dekker, New York, pp. 1–188.
70. V. J. Hruby and H. I. Mosberg (1981) in D. H. Schlesinger (Ed.), *Neurohypophyseal Peptide Hormones and Other Biological Active Peptides*, Elsevier North-Holland, Amsterdam, pp. 227–237.
71. V. J. Hruby (1981) in A. S. V. Burgen and G. C. K. Roberts (Eds.), *Topics in Molecular Pharmacology*, North-Holland, Amsterdam, p. 100.
72. V. J. Hruby, D. A. Upson, D. M. Yamamoto, C. W. Smith, and R. Walter (1979) *J. Am. Chem. Soc.* **101**, 2717–2721.
73. R. J. Turner, J. M. Matsoukas, and G. J. Moore (1990) *Biochem. Biophys. Res. Comm.* **171**, 996–1001.
74. N. J. Turro (Ed.) (1978) *Modern Molecular Photochemistry*, Benjamin Cummings, Inc., pp. 305–311.
75. D. D. Eads, B. G. Dismer, and G. R. Fleming (1990) *J. Chem. Phys.* **93**, 1136–1148.
76. J. Kusba and B. Sipp (1988) *Chem. Phys.* **124**, 223–226.
77. J. R. Lakowicz et al, submitted for publication.